Preparation of highly active unsupported Ni–Si–Mo catalyst for the deep hydrogenation of aromatics

Changlong Yin, Tongtong Wu, Chengwu Dong, Fan Li, Dong Liu, Chenguang Liu

PII: S0925-8388(20)31439-0

DOI: https://doi.org/10.1016/j.jallcom.2020.155076

Reference: JALCOM 155076

To appear in: *Journal of Alloys and Compounds*

Received Date: 24 November 2019

Revised Date: 16 March 2020

Accepted Date: 5 April 2020

Please cite this article as: C. Yin, T. Wu, C. Dong, F. Li, D. Liu, C. Liu, Preparation of highly active unsupported Ni–Si–Mo catalyst for the deep hydrogenation of aromatics, *Journal of Alloys and Compounds* (2020), doi: https://doi.org/10.1016/j.jallcom.2020.155076.

Credit Author Statement

Authors' individual contributions

Changlong Yin: Conceptualization, Data curation, Investigation, Methodology, Writing-Original Draft.

Tongtong Wu: Data curation, Formal analysis, Validation, Visualization, Writing-original draft.

Chengwu Dong: Formal analysis, Validation, Visualization.

Fan Li: Formal analysis, Validation, Visualization.

Dong Liu: Writing-Review & Editing.

Chenguang Liu: Writing-Review & Editing.

Preparation of highly active unsupported Ni-Si-Mo catalyst for the deep hydrogenation of aromatics

Changlong Yin*, Tongtong Wu, Chengwu Dong, Fan Li, Dong Liu, Chenguang Liu

(State Key Laboratory of Heavy Oil Processing and Key Laboratory of Catalysis of CNPC, China University of Petroleum, Qingdao 266580, P. R. China)

Corresponding Author: yincl@upc.edu.cn (Changlong Yin); TEL: +86-532-86984629

ABSTRACT A mesoporous nickel-silicon-molybdenum composite oxide with the phase of ammonium nickel (or silicon) molybdate was synthesized by chemical precipitation and unsupported nickel-silicon-molybdenum sulfide catalysts with various Ni/Si ratios were obtained by sulfidation of the oxide precursors. The oxide precursors and unsupported sulfide catalysts were characterized by XRD, N_2 adsorption-desorption, SEM, TPR, and HRTEM. The unsupported nickel-silicon-molybdenum sulfide catalysts were tested in the hydrogenation of naphthalene. It was found that the introduction of Si could increase the specific surface area and improve the pore structure of precursors, and reduce the reduction temperature of Mo species. The results of naphthalene hydrogenation showed that the introduction of Si could significantly improve the hydrogenation activity of the catalysts, especially the Ni9.5Si0.5Mo10 catalyst exhibited the highest aromatic hydrogenation activity at low temperature. Interestingly, it is found that the tetralin selectivity is 100 % in the low temperature range (220-260 °C) over Si10Mo10 catalyst, which might be attractive in the production of tetralin and other industrial application.

Keywords nickel-silicon-molybdenum composite oxide; unsupported nickel-silicon-molybdenum sulfide catalysts; naphthalene; hydrogenation activity

1. Introduction

High content of aromatics in distillates such as diesel, gasoline and jet fuel will reduce the quality of fuel [1] and produce harmful exhaust gases such as PM2.5 and NOx that pollute the environment [2-4]. Meanwhile, these aromatics and the resulting emissions are potentially dangerous and carcinogenic [5]. Therefore, increasingly stringent environmental regulations and fuel codes require the reduction of aromatics in fuels [6]. It can be seen that deep dearomatization has become an important issue in the production of clean fuels, and it is imperative to develop the production technology of ultra-clean fuel for efficient dearomatization.

Traditional industrial hydrotreating processes can simultaneously remove S and N by hydrodesulfurization (HDS) and hydrodenitrogenation (HDN) reactions. The current hydrotreating process is also applicable to hydrodearomatization (HDA). FCC diesel contains a large number of aromatics, most of which contain bicyclic aromatics of more than 50%. However, aromatics are the root cause of poor combustion performance and high density of FCC diesel oil [7-9]. FCC diesel has a high content of monocyclic aromatics through the conventional hydrofining method, which is mainly due to the relative ease of partial hydrogenation and saturation reactions of the polycyclic aromatics. However, the hydrogenation of monocyclic aromatics can be completely saturated by catalysts with high hydrogenation activity. High temperature is needed to catalyze the hydrogenation of aromatics if we use the traditional

supported metal sulfide system, but kinetically, the high temperature is not conducive to the hydrogenation of aromatics. The unsupported catalyst has no support, which greatly increases the content of active components and makes the catalyst have higher catalytic activity. Moreover, the unsupported catalyst has a strong catalytic hydrogenation activity also depends on its high resistance to S, N poisoning [10, 11]. However, the unsupported catalyst has problems such as small specific surface area and small pore size, which is not suitable for catalyzing the hydrogenation reaction of macromolecular polycyclic aromatics. Therefore, further research is needed on how to obtain a highly active unsupported catalyst with a high specific surface area and good pore structure.

Pang et al [12] prepared Mo_2C/AC transition metal carbide catalyst with different load by microwave radiation method using activated carbon (AC) as the carrier. The catalyst 20 wt.%-Mo_2C/AC can make the selectivity of tetralin up to 100 % and the conversion rate of naphthalene up to 95 %. The activated carbon carrier is very important for the catalyst to obtain high activity and good stability. Liang et al [13] successfully synthesized CoSi/SiO_2 catalyst in a fluidized bed using $Co(SiCl_3)(Co)_4$ as the precursor by the MOCVD method, which has high aromatic hydrogenation activity and selectivity of 100% for the hydrogenation of naphthalene into tetralin. In the relatively short contact time between naphthalene and catalyst (3.76 min), the reaction of further hydrogenation of tetralin to decalin did not occur, which indicates that the hydrogenation of tetralin is the rate control step of catalytic hydrogenation of naphthalene. Under the same reaction conditions, the naphthalene hydrogenation

reaction catalyzed by the contrast catalyst Co/SiO_2 did not get any product, which means that the activity of $CoSi/SiO_2$ catalyst is higher than that of Co/SiO_2 catalyst. The results show that the introduction of Si into transition metals can produce novel catalysts of aromatic hydrogenation, which are expected to be used in petroleum processing. Thermodynamic calculation shows that the transition metal silicides can tolerate higher H_2S concentration than the corresponding carbides and nitrides [14], which means that the introduction of Si in the transition metal catalyst is more stable and sulfur-tolerant in the reaction of sulfur-containing compounds.

Therefore, unsupported NiSiMo catalysts with different Ni/Si molar ratios were synthesized by chemical precipitation method. The effects of the addition of Si on the physicochemical properties of unsupported NiMo catalysts and the hydrogenation performance of aromatics were investigated. Since the proportion of bicyclic aromatics in FCC diesel is the highest, the hydrogenation saturation of bicyclic aromatics is mainly studied. In scientific research, naphthalene is generally used as a model compound to study the hydrogenation of bicyclic aromatics [15-17]. Therefore, the hydrogenation activity evaluation of the unsupported catalyst prepared in this paper was carried out by using naphthalene as a model compound.

2. Experimental

2.1. Preparation of unsupported NiSiMo catalyst

A solution of 0.1 mol ammonium molybdate, a certain amount of nickel nitrate and tetraethyl silicate was dissolved in a 500 mL three-necked, round-bottomed flask. The solution was heated to 90 °C. Then ammonia water was added in drops until the

solution pH was about 12. The green precipitate (the precursor of Si10Mo10 was white precipitate) was produced by heating at a constant temperature for 12 h. The precipitate was isolated by vacuum filtration and dried for 12 h at 100 °C to obtain the powder catalyst precursor. According to the different molar ratios of Ni/Si, the prepared catalysts were named NixSiyMo10, where x and y were the molar ratios of Ni and Si added in the preparation, and the molar ratio of (Ni+Si)/Mo was always maintained at 1:1.

2.2. Characterization of the catalyst

2.2.1 X-ray diffraction (XRD)

The crystal phase of the catalysts was measured by X-ray diffraction (XRD) on an X'Pert Pro MPD instrument with Cu Kα. The scanning angle was 5-75^{o}, the scanning speed was 5^{o}·min^{-1}, and the step speed was 0.0001°. The detector was a scintillation counter with a tube pressure of 45 kV and a current of 40 mA. Before the measurement, the sample was ground into powder and pressed into a smooth sheet.

2.2.2 Low temperature N_2 adsorption-desorption (BET)

The pore structure properties of the samples were determined by using the ASAP 2010 automatic adsorption apparatus (Micromeritics, USA). The samples were processed at 300 °C in vacuum before the measurement, and the N_2 adsorption-desorption temperature was -196 °C. The specific surface area was obtained by the BET method, the pore volume was calculated by the BJH method, and the average pore size was calculated by the desorption curve. All samples were calcined at 300 °C for 4 h for pretreatment before measuring the pore structure

properties.

2.2.3 Scanning electron microscopy (SEM)

The morphology analysis of the samples was carried out by S-4800 cold field emission scanning electron microscope (Hitachi Company, Japan). The X650 scanning electron microscope was vacuumized for 25-30 min, and the sample was put into the sample chamber after the vacuum degree of the instrument reached above 1×10^{-4} Pa, the operating voltage was 5.0 kV and the working distance was 8.2 mm, and then the surface structure of the sample was observed.

2.2.4 High-resolution transmission electron microscope (HRTEM)

The morphology of the sulfided catalysts was observed by a JEM-2100UHR high-resolution transmission electron microscope (JEOL Company, Japan) operated at 200 kV. The sulfided catalysts were stored and ground in ethanol to avoid oxidation due to exposure to air. After grinding, the sample was thoroughly dispersed in ethanol by ultrasound for 30 min, and then a small amount of upper suspension was taken for observation.

2.2.5 Temperature programmed reduction (TPR)

The reduction performance of the samples was performed on a CHEMBET-3000 TPR Analyzer. The sample loading quantity was 0.05 g, and the size of the sample was 20-40 mesh. The reduced gas was H_2/Ar with a volume fraction of 10 % and a gas flow rate of 80 $mL\cdot min^{-1}$. During the heating process, the hydrogen consumption of the sample was recorded with a thermal conductivity detector (TCD). The rate of heating was 10 □·min^{-1} and the temperature was raised to 900 °C.

2.3. Catalyst activity evaluation

The aromatic hydrogenation performance of unsupported catalysts was evaluated by a 10 mL fixed bed high pressure hydrogenation micro-reactor. 5 mL of 20-40 mesh catalyst particles were packed into the middle of the reaction tube, and the upper and lower ends of the reaction tube were filled with quartz sand of the same particle size. Before the evaluation of the aromatic hydrogenation activity of the unsupported catalyst was started, the oxide precursor was in situ presulfided using a 3.0 wt% CS_2/petroleum ether solution at 330 °C for 8 h at a H_2 pressure of 3 MPa, and a liquid hourly space velocity (LHSV) of 2 h^{-1}. The aromatic hydrogenation activity of the catalyst was evaluated using an 8.0 wt% naphthalene/petroleum ether solution as the feed oil. The reaction conditions were: reaction temperatures of 220°, 240, 260, 280, 300 and 320 °C, a reaction pressure 3 MPa, a liquid hourly space velocity of 2 h^{-1}, a H_2/oil ratio of 400:1. The product distribution of naphthalene hydrogenation was analyzed by a GC-7820 gas chromatograph.

3. Results and discussion

3.1. Characterization of oxidic NiSiMo precursor

Figure 1 shows the XRD characterization results of the NiSiMo precursors with different Ni/Si molar ratios. The characteristic diffraction peaks of ammonium nickel molybdate crystals are found in the samples Ni10Mo10, Ni9.5Si0.5Mo10, Ni8Si2Mo10 and Ni5Si5Mo10 ($(NH_4)HNi_2(OH)_2(MoO_4)_2$, JCPDS card No.50-1414) [18]. However, the diffraction peaks are not found in the sample Si10Mo10, which is almost in an amorphous or microcrystalline state. The introduction of Si will change

the crystal structure of ammonium nickel molybdate of the original NiMo precursor. With the increase of the amount of Si introduced, the characteristic diffraction peak intensity of the ammonium nickel molybdate crystal phase gradually weakens until it disappears into an amorphous or microcrystalline structure. Besides, the diffraction peaks of Si species are not detected in the XRD patterns, which may be caused by the high dispersion of Si species in the precursors.

(Figure 1.)

The N_2 adsorption-desorption isotherms and pore size distributions of the NiSiMo precursors are shown in Figure 2. It can be seen from Figure 2(a) that the low-temperature N_2 adsorption-desorption curves of the NiSiMo precursors with different Ni/Si molar ratios are all Type IV [19], indicating that the NiSiMo precursors are mesoporous materials. From the pore size distributions of the NiSiMo precursors (Figure 2b), it can be found that the pore size distribution of the Si10Mo10 precursor is wider than that of other NiSiMo precursors. The pore size of the Si10Mo10 precursor is distributed from less than 2 nm to 70 nm. The pore size distributions of the Ni10Mo10, Ni9.5Si0.5Mo10, Ni8Si2Mo10 and Ni5Si5Mo10 precursors are narrow, and the most probable pore sizes are 3.74, 3.58, 3.91 and 3.90 nm respectively.

(Figure 2.)

The pore properties of the NiSiMo precursors are summarized in Table 1. The pore structure is an important factor affecting the catalytic activity. The higher specific surface area is beneficial to the uniform distribution of hydrogenation active sites on

the surface of the catalyst, which is favorable for the continuous hydrogenation reactions. Clearly, as the amount of Si introduced increases, the specific surface area of the NiSiMo precursors also increases. Compared with the Ni10Mo10 precursor, the pore size of the Ni8Si2Mo10 precursor decreases, and the pore sizes of the Ni9Si0.5Mo10, Ni5Si5Mo10, and Si10Mo10 precursors increase.

(Table 1.)

Shown in Figure 3 are the SEM images of the NiSiMo precursors. The Ni10Mo10 precursor contains many irregular bulk structures of 200-1000 nm, on which some spherical particles of about 30 nm adhere. The Ni9.5Si0.5Mo10 precursor also has a bulk structure similar to the Ni10Mo10 precursor, but the size of about 300-800 nm is smaller than the Ni10Mo10 precursor, and more small particles of less than 50 nm are attached to the bulk structure. In addition to bulk crystals, the Ni8Si2Mo10 precursor also have flower-like structures, which are formed by the self-assembly of nano-spherical structures. The Ni5Si5Mo10 precursor is similar to the Ni8Si2Mo10 precursor, it can be clearly seen that the large bulk structure formed by the accumulation of nanoparticles, and the nano-spherical structures adhere to the bulk crystals. The morphological structure of the Si10Mo10 precursor is mainly transformed into small particles with a relatively uniform dispersion of about 20 nm. It can be seen that with the increase of the amount of Si introduced, the bulk structure of the precursor gradually disappears, and the nano-spherical structure adheres to the large bulk crystals, and then gradually transforms into the nano-spherical particles. The results further validate the XRD characterization results, as the amount of Si

increases, the peak intensity of the ammonium nickel molybdate gradually weakens until it transforms into an amorphous or microcrystalline structure similar to that of the Si10Mo10 precursor.

(Figure 3.)

The TPR profiles of the NiSiMo precursors are presented in Figure 4. It is generally considered that the Ni10Mo10 precursor shows only a large and broad reduction peak in the range of 400-690 °C, and the other NiSiMo precursors have two reduction peaks. According to the literature reports, the reduction peak in the range of 400 °C to 690 °C should be attributed to the reduction of Mo species with octahedral coordination, that is, the reduction of Mo^{6+} to Mo^{4+} [20]. The reduction peak at 750 °C to 900 °C can be ascribed to the reduction of Mo species with tetrahedral coordination, that is, the reduction of Mo^{4+} to the metal Mo^{0} [21, 22]. The reduction temperature is above 800 °C, which is due to the difficult reduction of the Mo species with tetrahedral coordination [23, 24]. As can be seen from the figures that the introduction of Si can reduce the reduction temperature of Mo species, and the reduction temperature of the Mo species decreases as the amount of Si increases. It has been proved that the introduction of Ni species could make the reduction of Mo species easier [25]. The reduction peaks of Ni species easily overlap with those of Mo species, making it difficult to distribute the reduction temperature of Ni species [20]. However, there are some differences in the intensities of reduction peaks. The intensities of reduction peaks of the Ni10Mo10, Ni9.5Si0.5Mo10, Ni8Si2Mo10, and Ni5Si5Mo10

precursors are significantly greater than those of the Si10Mo10 precursor, which may be due to the overlap of the Ni and Mo signals in the precursors.

(Figure 4.)

3.2 Characterization of sulfided NiSiMo catalysts

The XRD patterns of the sulfided unsupported NiSiMo catalysts are displayed in Figure 5, from which we can find that the characteristic diffraction peaks of the MoS_2 and Ni_3S_2 crystal phases are detected in the sulfided NiSiMo catalysts [26, 27]. As the amount of Si increases in the catalysts, the peak intensities of the MoS_2 and Ni_3S_2 crystal phases decrease. The average crystal sizes of Ni_3S_2 and MoS_2 in the sulfided catalysts calculated by the Scherrer equation are shown in Table 2. It can be concluded from the results that the average crystal size of Ni_3S_2 phase and MoS_2 phase gradually decreases with the increase of the amount of Si introduced, which is consistent with the XRD characterization results. Although the nickel content on the catalysts is different, the molybdenum content on the five catalysts is basically the same, which indicates that the introduction of Si contributes to the dispersion of active metal components in the catalysts, thereby making the NiSiMo catalysts have good potential for aromatic hydrogenation.

(Figure 5 and **Table 2**)

The N_2 adsorption-desorption isotherms and pore size distributions of the sulfided NiSiMo catalysts are depicted in Figure 6. It can be observed that the adsorption and desorption curves of the sulfided NiSiMo catalysts are all Type IV, which is a typical characteristic of mesoporous materials. The pore size distributions of the sulfided

Ni9.5Si0.5Mo10 and Ni8Si2Mo10 catalysts are narrow, and the pore size distributions of the sulfided Ni10Mo10 and Ni5Si5Mo10 catalysts are relatively wide. Obviously, the sulfided Si10Mo10 catalyst has a very wide pore size distribution.

(Figure 6.)

Table 3 shows the pore properties of the sulfided NiSiMo catalysts. Compared with Table 1, it can be found that except for the Ni5Si5Mo10 precursor, the specific surface area of other NiSiMo precursors increases after sulfurization. The pore volume of Ni10Mo10 precursor increases after sulfurization, and the pore volume of other sulfided NiSiMo catalysts is basically unchanged. Meanwhile, the pore size of the Ni10Mo10 and Ni5Si5Mo10 precursors increases, and the pore size of other NiSiMo precursors decreases after sulfurization.

(Table 3.)

The microstructure of the active components in the sulfided catalysts was investigated by HRTEM. The results are shown in Figure 7. As seen by the images, the black stripes with a spacing of about 0.6 nm are found in the HRTEM images of all catalysts, which can be attributed to the structure of the MoS_2 crystal [28, 29]. The hydrogenation activity of the sulfided NiMo catalyst is also related to the slab length and the stacking layer number of MoS_2 [30]. The shorter slab length and the more stacking layer number can produce higher hydrogenation activity [31-33]. The Ni_3S_2 fringes with a spacing of about 0.29 nm are also detected for the Ni10Mo10 and Ni9.5Si0.5Mo10 catalysts [34]. The length of the MoS_2 nanoparticle layer in the sulfided Ni10Mo10 catalyst is longer than those of the other sulfided catalysts, and

the stacking numbers of the MoS_2 layers of the Si10Mo10 catalyst are lower than those of the other NiSiMo catalysts, which are consistent with the XRD results of the sulfided NiSiMo catalysts. The MoS_2 observed in the sulfided Ni9.5Si0.5Mo10 catalysts is more striped, indicating that the Ni9.5Si0.5Mo10 catalyst will have higher hydrogenation activity. On the whole, the dispersion of MoS_2 increases with the increase of silicon content in the catalysts.

(Figure 7.)

3.3. Evaluation of aromatic hydrogenation activity of unsupported NiSiMo catalysts

3.3.1. Activity evaluation of the NiSiMo catalysts

The conversion rate of naphthalene hydrogenation reaction on the unsupported NiSiMo catalysts is shown in Figure 8(a). The selectivity of decalin on the unsupported NiSiMo catalysts is shown in Figure 8(b). In the range of 220-320 °C, the conversion of naphthalene hydrogenation reaction increases first and then decreases slowly, and the NiSiMo catalysts can reach a high conversion rate (> 99.8 %). The hydrogenation conversion rate of naphthalene on the NiSiMo catalysts exceeded 98.61 % in the temperature range of 220-260 °C, which was significantly higher than that of the Ni10Mo10 catalyst. This indicates that the introduction of Si can significantly improve the naphthalene hydrogenation activity of the unsupported NiMo catalyst, especially the low temperature aromatic hydrogenation performance of the catalyst (220-260 °C). In addition, Figure 8(b) shows that the selectivity of decalin increases with the increase of reaction temperature, indicating that the temperature is beneficial to obtain more decalin on the sulfided NiSiMo catalyst. On the other hand,

the selectivity of decalin decreases in the order of Ni10Mo10 > Ni9.5Si0.5Mo10 > Ni8Si2Mo10 > Ni5Si5Mo10, indicating that the selectivity of decalin gradually decreases with the increase of the amount of Si introduced, and the introduction of Si is not beneficial for the conversion of naphthalene into decalin. Catalysts with different content of Si have different aromatic hydrogenation activities. The Ni9.5Si0.5Mo10 catalyst has the highest aromatic hydrogenation activity, the conversion of naphthalene hydrogenation is 100 % and the selectivity of decalin is 68.81 % at 260 °C, which is slightly lower than that of the Ni10Mo10 catalyst (69.61 %). The high aromatic hydrogenation activity of the Ni9.5Si0.5Mo10 catalyst is closely related to the physicochemical characteristics of the sulfided catalysts. The XRD results of the sulfided catalysts showed that compared with other NiSiMo catalysts, the sulfided Ni9.5Si0.5Mo10 catalyst had higher crystallinity MoS_2 and Ni_3S_2 crystal phases. HRTEM showed that there were more clutter-stacked MoS_2 nanoparticles in the sulfided Ni9.5Si0.5Mo10 catalyst. These properties can make the Ni9.5Si0.5Mo10 catalyst has higher aromatic hydrogenation activity.

(Figure 8.)

3.3.2. Activity evaluation of the Si10Mo10 catalyst

The conversion of naphthalene hydrogenation reaction, the selectivity of decalin and the selectivity of tetralin of the Si10Mo10 catalyst are shown in Figure 9. The conversion of naphthalene hydrogenation of the Si10Mo10 catalyst increases remarkably with the increase of reaction temperature, the conversion rate is only 4.71 % at 220 °C and 72.3 % at 320 °C, but it is still significantly lower than other NiSiMo

catalysts. In addition, the Si10Mo10 catalyst is not conducive to the deep hydrogenation of naphthalene, and its decalin selectivity is almost 0. However, it has a very high selectivity of tetralin, and the tetralin selectivity is 100 % in the low temperature range (220-260 °C). In summary, the Si10Mo10 catalyst can be used as a selective hydrogenation of naphthalene to produce tetralin. At 320 °C, the naphthalene conversion rate of the Si10Mo10 catalyst is 71.97 %, and the selectivity of tetralin is 98.95 %.

(Figure 9.)

4. Conclusion

A series of NiSiMo precursors with different Ni/Si molar ratios were synthesized by chemical precipitation method. The results showed that the introduction of Si in the unsupported catalysts could increase the specific surface area of the catalysts, and decrease the average grain size of MoS_2 and Ni_3S_2. The results of naphthalene hydrogenation evaluation showed that the introduction of Si could significantly improve the naphthalene hydrogenation activity of the unsupported catalyst, especially the low temperature aromatic hydrogenation performance of the catalyst (220-260 °C). The Ni9.5Si0.5Mo10 catalyst exhibited the highest aromatic hydrogenation activity, and the Si10Mo10 catalyst was not conducive to deep hydrogenation of naphthalene, but it had a very high selectivity of tetralin (about 100 %).

Acknowledgements

This work was financially supported by the National Natural Science Fund of China (Grant No. 21676301), the National key R & D program of China (2017YFB0602500). Financial support from the program of China Scholarships Council (No.201806455007) and Petro China Corporation Limited was also greatly appreciated.

References

[1] T. Tang, C. Yin, L.Wang, Good sulfur tolerance of a mesoporous Beta zeolite supported palladium catalyst in the deep hydrogenation of aromatics, Journal of Catalysis 257 (2008) 125-133.

[2] M.A. Vicerich, M. Oportus, V.M. Benitez, Influence of Na content on the catalytic properties of Pt-Ir/Al_2O_3 catalysts for selective ring opening of decalin, Applied Catalysis A: General 480 (2014) 42-49.

[3] G.N. Yun, Y.K. Lee, Dispersion effects of Ni_2P catalysts on hydrotreating of light cycle oil, Applied Catalysis B Environmental 150 (2014) 647-655.

[4] A.C.A. Monteiro-Gezork, A. Effendi, J.M. Winterbottom, Hydrogenation of naphthalene on NiMo- and Ni/Al_2O_3 catalysts: Pre-treatment and deactivation, Catalysis Today 128 (2007) 63-73.

[5] A.Rubio-Clemente, R.A Torres-Palma, G.A. Peñuela, Removal of polycyclic aromatic hydrocarbons in aqueous environment by chemical treatments: A review, Science of the Total Environment 478 (2014) 201-225.

[6] A. Zhao, X. Zhang, X. Chen, Cobalt Silicide Nanoparticles in Mesoporous Silica

as Efficient Naphthalene Hydrogenation Catalysts by Chemical Vapor Deposition, Journal of Physical Chemistry C 114 (2010) 3962-3967.

[7] L. Wang, B. Shen, F. Fang, Upgrading of light cycle oil via coupled hydrogenation and ring-opening over NiW/Al2O3 -USY catalysts, Catalysis Today 158 (2010) 343-347.

[8] Y. Choi, J. Lee, J. Shin, Selective hydroconversion of naphthalenes into light alkyl-aromatic hydrocarbons, Journal of Solid State Electrochemistry 492 (2015) 140-150.

[9] C. Peng, X.C. Fang, R.H. Zeng, Commercial analysis of catalytic hydroprocessing technologies in producing diesel and gasoline by light cycle oil, Catalysis Today 276 (2016) 11-18.

[10] F.L. Plantenga, R. Cerfontain, S. Eijsbouts, "Nebula": A hydroprocessing catalyst with breakthrough activity, Studies in Surface Science & Catalysis 145 (2003) 407-410.

[11] S. Eijsbouts, S.W. Mayo, K. Fujita, Unsupported transition metal sulfide catalysts: From fundamentals to industrial application, Applied Catalysis A: General 322 (2007) 58-66.

[12] M. Pang, C. Liu, W. Xia, Activated carbon supported molybdenum carbides as cheap and highly efficient catalyst in the selective hydrogenation of naphthalene to tetralin, Green Chemistry 14 (2012) 1272-1276.

[13] C. Liang, A. Zhao, X. Zhang, CoSi particles on silica support as a highly active and selective catalyst for naphthalene hydrogenation, Chemical Communications 15 (2009) 2047-2049.

[14] R. Prins, Catalytic hydrodenitrogenation, Advances in Catalysis 46 (2001) 399-464.

[15] A.C.A. Monteiro-Gezork, R. Natividad, J.M. Winterbottom, Hydrogenation of naphthalene on NiMo- Ni- and Ru/Al_2O_3 catalysts: LangmuirHinshel-wood kinetic modelling, Catalysis Today 130 (2008) 471-485.

[16] M. Du, Z. Qin, H. Ge, Enhancement of $Pd\text{-}Pt/Al_2O_3$ catalyst performance in naphthalene hydrogenation by mixing different molecular sieves in the support, Fuel Processing Technology 91(2010) 1655-1661.

[17] S. Ren, P. Zhang, H. Shui, Promotion of Ni/SBA-15 catalyst for hydrogenation of naphthalene by pretreatment with ammonia/water vapour, Catalysis Communications 12 (2010) 132-136.

[18] D. Levin, S.L. Soled, J.Y. Ying, ChemInform Abstract: Crystal Structure of an ammonium Nickel Molybdate prepared by Chemical Precipitation, ChemInform 35 (14) (1996) 4191-4197.

[19] S.L. Amaya, G.Alonso-Núñez, T.A.Zepeda, Effect of the divalent metal and the activation temperature of NiMoW and CoMoW on the dibenzothiophene hydrodesulfurization reaction, Applied Catalysis B: Environmental 148-149 (2014) 221-230.

[20] C. F. Linares, M. Fernández, Study of the Individual Reactions of Hydrodesulphurization of Dibenzothiophene and Hydrogenation of 2-Methylnaphthalene on ZnNiMo/γ-Alumina Catalysts, Catalysis Letters 126 (3-4) (2008) 341-345.

[21] J. Zhang, Z. Xin, X. Meng, Effect of MoO_3 on the heat resistant performances of nickel based MCM-41 methanation catalysts, Fuel 116 (2014) 25-33.

[22] C. F. Linares, J. López, A. Scaffidi, Preparation of ZnNiMo/γ-alumina catalysts from recycled Ni for hydrotreating reactions, Applied Catalysis A General 292 (2005) 113-117.

[23] S. Garg, K. Soni, T. A. Prabhu, Effect of ordered mesoporous Zr SBA-15 support on catalytic functionalities of hydrotreating catalysts 2. Variation of molybdenum and promoter loadings, Catalysis Today 261 (2016) 128-136.

[24] H. Liu, Y. Li, C. Yin, Preparation of highly active unsupported nickel–zinc–molybdenum catalysts for the hydrodesulfurization of dibenzothiophene, Applied Catalysis B Environmental 174-175 (2015) 264-276.

[25] H. Liu, Y. Li, C. Yin, One-pot synthesis of ordered mesoporous NiMo-Al_2O_3 catalysts for dibenzothiophene hydrodesulfurization, Applied Catalysis B: Environmental 198 (2016) 493-507.

[26] C. Yin, Y. Wang, S. Xue, Influence of sulfidation conditions on morphology and hydrotreating performance of unsupported Ni-Mo-W catalysts, Fuel 175 (2016) 13-19.

[27] H. Liu, C. Yin, B. Liu, Effect of Calcination Temperature of Unsupported NiMo Catalysts on the Hydrodesulfurization of Dibenzothiophene, Energy & Fuels 28 (2014) 2429-2436.

[28] Y. Gochi, C. Ornelas, F. Paraguay, S. Fuentes, L. Alvarez, J.L. Rico, G. AlonsoNúñez, Effect of sulfidation on Mo-W-Ni trimetallic catalysts in the HDS of DBT, Catalysis Today 107 (2005) 531-536.

[29] C. Yin, L. Zhao, Z. Bai, H. Liu, Y. Liu, C. Liu, A novel porous ammonium nickel molybdate as the catalyst precursor towards deep hydrodesulfurization of gas oil, Fuel 107 (2013) 873-878

[30] X. Liu, X. Li, Z. Yan, Facile route to prepare bimodal mesoporous γ-Al_2O_3 as support for highly active CoMo-based hydrodesulfurization catalyst, Applied Catalysis B: Environmental 1211-22 (2012) 50-56.

[31] R.Y. Zhao, L.Y. Zeng, J. Liang, C.G. Liu, Interaction between Ni promoter and Al_2O_3 support and its effect on the performance of NiMo/γ-Al_2O_3 catalyst in hydrodesulphurization, Journal of Fuel Chemistry and Technology 44 (2016) 564-569.

[32] L. Vradman, M.V. Landau, Structure-Function Relations in Supported Ni-W Sulfide Hydrogenation Catalysts, Catalysis Letters 77 (2001) 47-54.

[33] E.J.M. Hensen, P.J. Kooyman, Y.V.D. Meer, A.M.V.D. Kraan, V.H.J.D. Beer, J.A.R.V. Veen, R.A.V. Santen, The Relation between Morphology and Hydrotreating Activity for Supported MoS2 Particles, Journal of Catalysis 199 (2001) 224-235.

[34] G. Ali, B.A. Korgel, Nickel sulfide and copper sulfide nanocrystal synthesis and polymorphism, Langmuir 21 (2005) 9451-9456.

Table 1. Pore properties of the NiSiMo precursors

Table 2. Average crystal sizes of Ni_3S_2 and MoS_2 in the sulfided NiSiMo catalysts

Table 3. Pore properties of the sulfided NiSiMo catalysts

Table 1. Pore properties of the NiSiMo precursors

NiMo precursor	S_{BET}[a] (m^2/g)	V_P[b] (cm^3/g)	D_P[c] (nm)
Ni10Mo10	31	0.06	6.26
Ni9.5Si0.5Mo10	30	0.11	8.94
Ni8Si2Mo10	69	0.04	5.74
Ni5Si5Mo10	71	0.03	7.37
Si10Mo10	122	0.62	18.96

a S_{BET}: BET surface area.

b V_P: Pore volume was calculated by the BJH method.

c D_p: Average pore diameter was calculated by the BJH method from the desorption branch of the isotherms.

Table 2. Average crystal sizes of Ni_3S_2 and MoS_2 in the sulfided NiSiMo catalysts

Catalyst	Ni10Mo10	Ni9.5Si0.5Mo10	Ni8Si2Mo10	Ni5Si5Mo10	Si10Mo10
Ni_3S_2/nm	40.6	37.8	30.7	18.2	-
MoS_2/nm	32.5	30.1	24.3	15.6	5.8

Table 3. Pore properties of the sulfided NiSiMo catalysts

NiMo precursor	S_{BET} (m^2/g)	V_P (cm^3/g)	D_P (nm)
Ni10Mo10	60	0.15	8.72
Ni9.5Si0.5Mo10	77	0.10	5.96
Ni8Si2Mo10	87	0.05	4.84
Ni5Si5Mo10	10	0.02	11.86
Si10Mo10	126	0.61	18.75

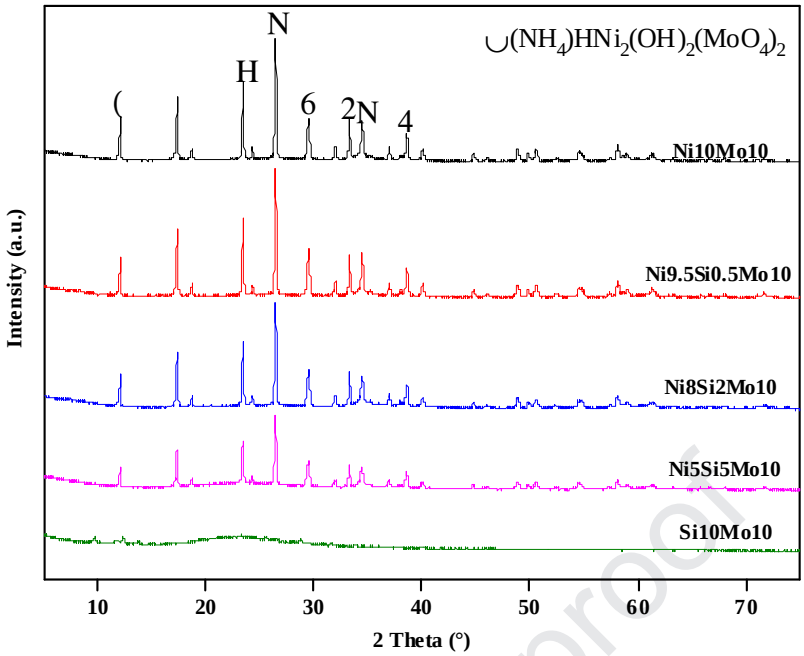

Fig. 1. XRD patterns of the NiSiMo precursors

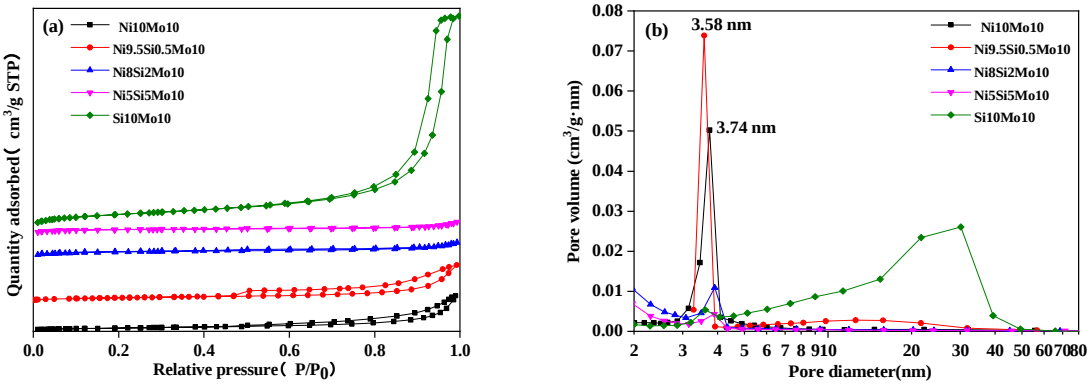

Fig. 2. N_2 adsorption-desorption isotherms (a) and pore size distributions (b) of the NiSiMo precursors

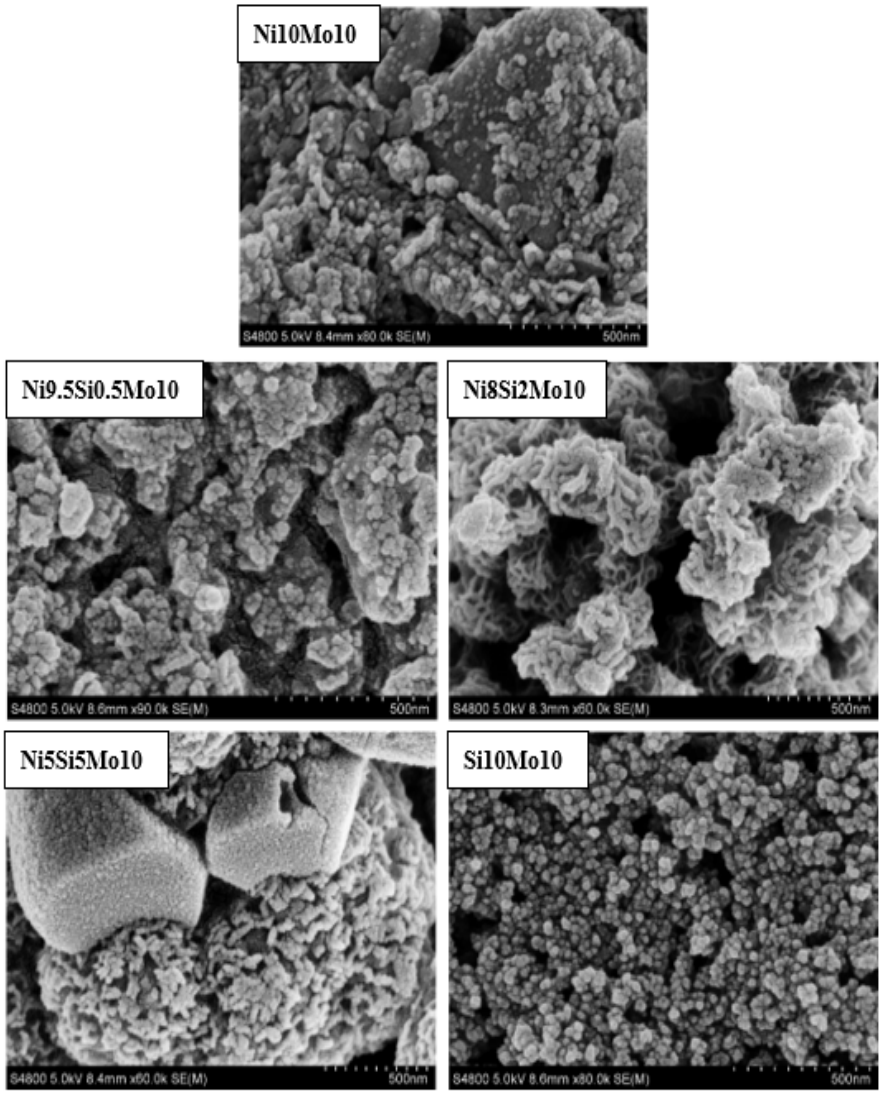

Fig. 3. SEM images of the NiSiMo precursors

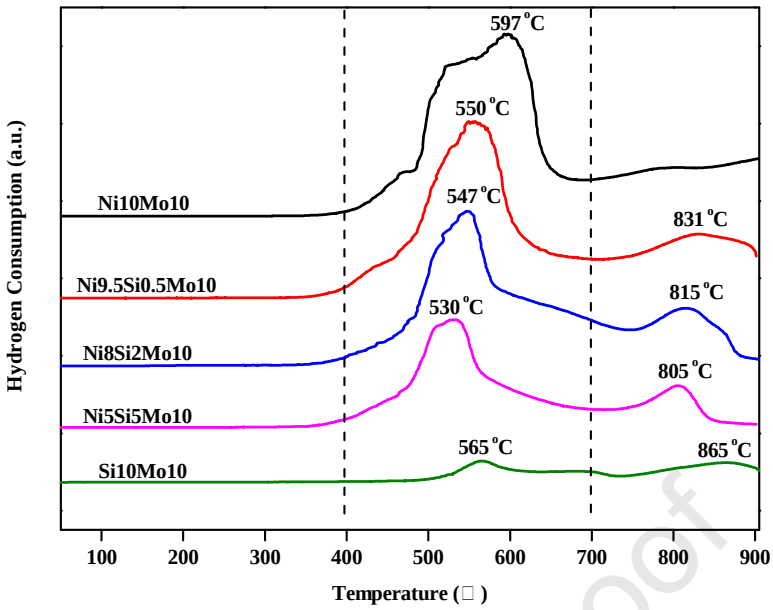

Fig. 4. TPR profiles of the NiSiMo precursors

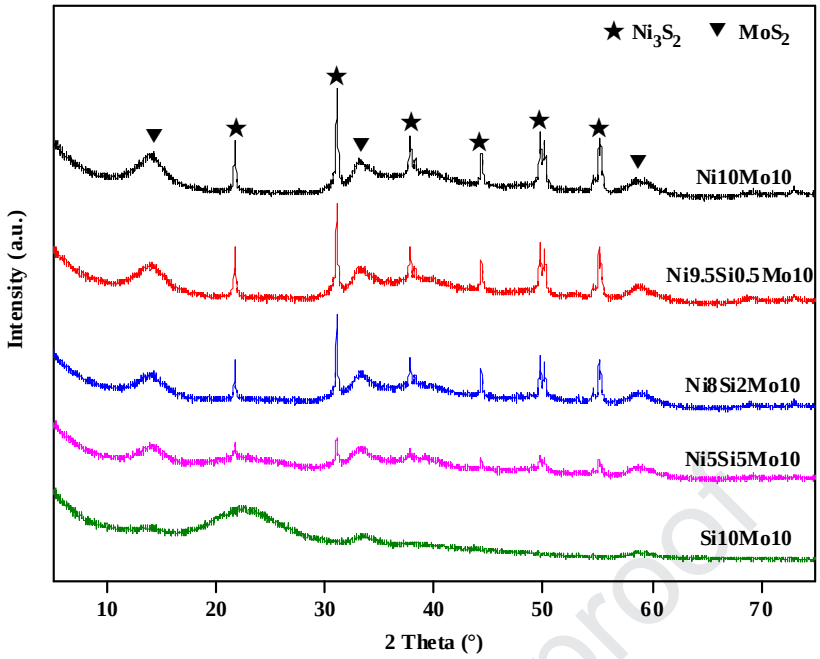

Fig. 5. XRD patterns of the sulfided NiSiMo catalysts

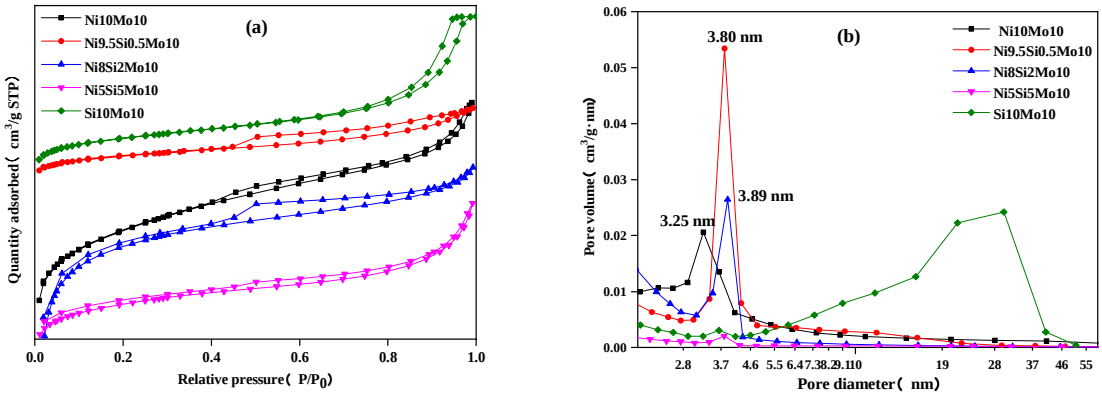

Fig. 6. N_2 adsorption-desorption isotherms (a) and pore size distributions (b) of the sulfided NiSiMo catalysts

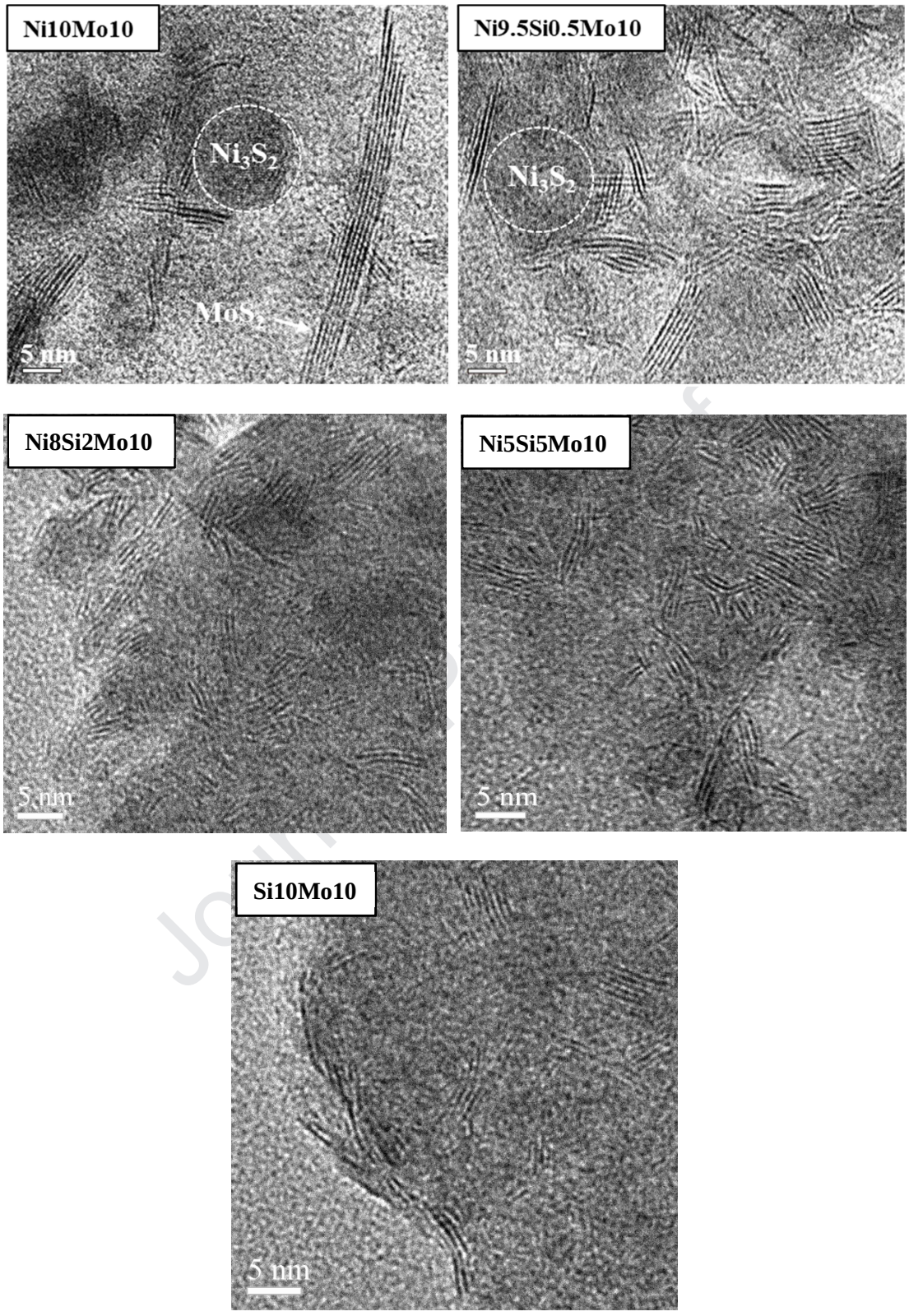

Fig. 7. HRTEM images of the sulfided NiSiMo catalysts

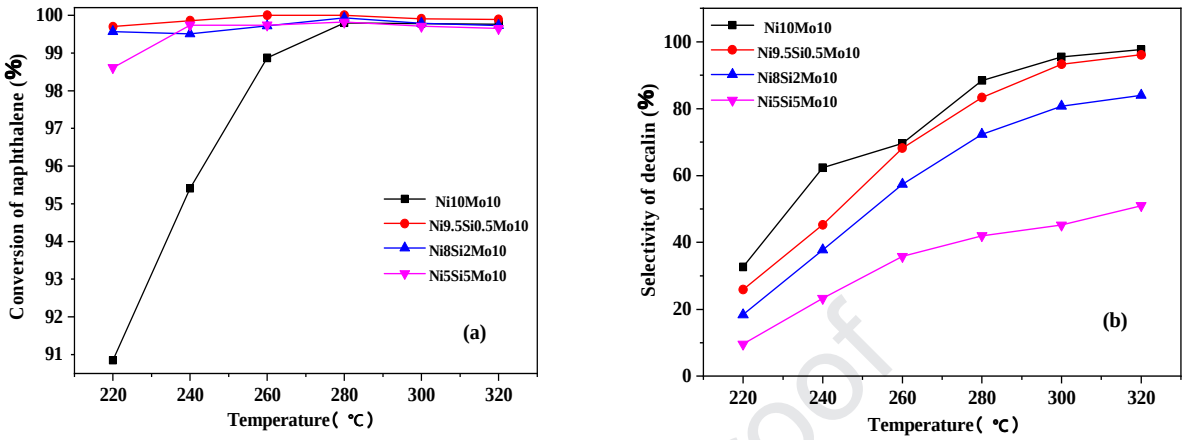

Fig. 8. The conversion rate of naphthalene hydrogenation (a) and the selectivity of decalin (b) on the unsupported NiSiMo catalysts

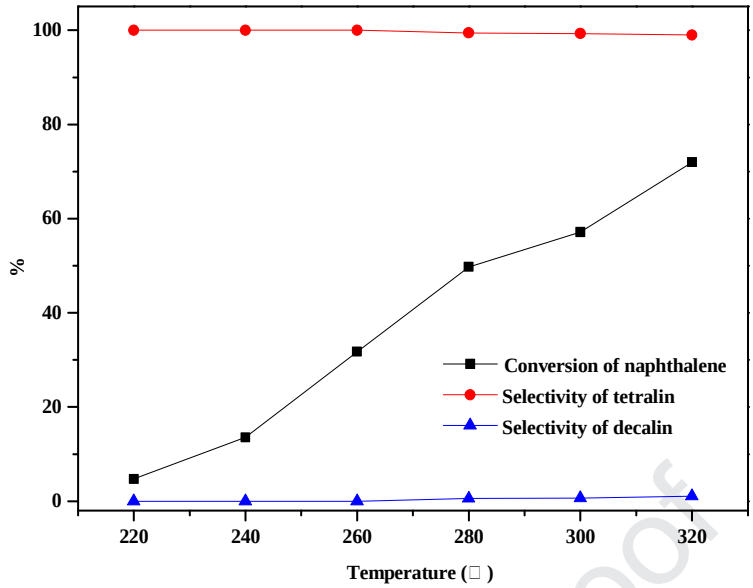

Fig. 9. Hydrogenation of naphthalene on the Si10Mo10 catalyst

The additive Si was introduced into an unsupported NiMo catalyst;

Pore propertie of unsupported catalyst was improved;

The reduction temperature of Mo species was reduced;

The hydrogenation activity was improved;

Declaration of interests

☐ The authors declare that they have no known competing financial interests or personal relationships that could have appeared to influence the work reported in this paper.